

Proximal Hamiltonian Monte Carlo

Apratim Shukla, Dootika Vats, and Eric C. Chi

Abstract—Bayesian formulation of modern day signal processing problems has called for improved Markov chain Monte Carlo (MCMC) sampling algorithms for inference. The need for efficient sampling techniques has become indispensable for high dimensional distributions that often characterize many core signal processing problems, e.g., image denoising, sparse signal recovery, etc. A major issue in building effective sampling strategies, however, is the non-differentiability of the underlying posterior density. Such posteriors are popular in models designed to recover sparse signals. As a result, the use of efficient gradient-based MCMC sampling techniques becomes difficult. We circumvent this problem by proposing a Proximal Hamiltonian Monte Carlo (p-HMC) algorithm, which leverages elements from convex optimization like proximal mappings and Moreau-Yosida (MY) envelopes within Hamiltonian dynamics. Our method improves upon the current state of the art non-smooth Hamiltonian Monte Carlo as it achieves a relatively sharper approximation of the gradient of log posterior density and a computational burden of at most the current state-of-the-art. A chief contribution of this work is the theoretical analysis of p-HMC. We provide conditions for geometric ergodicity of the underlying HMC chain. On the practical front, we propose guidance on choosing the key p-HMC hyperparameter – the regularization parameter in the MY-envelope. We demonstrate p-HMC’s efficiency over other MCMC algorithms on benchmark problems of logistic regression and low-rank matrix estimation.

Index Terms—Statistical Signal Processing, Hamiltonian Monte Carlo, Proximal Mapping, Moreau-Yosida Envelope, Sparse Logistic Regression, Low-Rank Matrix Estimation.

I. INTRODUCTION

MODERN computational power has paved the way for increasingly complex models in statistical signal processing [1]. Examples include models for compressed sensing [2], signal denoising [3]–[5], image denoising [6], image deconvolution [7], superresolution [8], [9], magnetic resonance image reconstruction [10], and computer vision [11], to name a few. A defining feature of these models is that they admit algorithms that recover low-dimensional characteristics from high-dimensional data. Within these model spaces, Bayesian models that employ sparsity inducing penalties furnish both point estimates of model parameters as well as desirable uncertainty estimates. Inference for Bayesian signal processing models depends on reliably generating samples from an often intractable posterior distribution. While generating independent and identically distributed (iid) samples from such complex and high-dimensional posterior distributions would be ideal, it is usually not possible beyond small dimensions. Fortunately, we can generate samples using a Markov chain whose stationary and limiting distribution coincides with our

desired posterior distribution via Markov chain Monte Carlo (MCMC) methods [12], [13]. These methods have found widespread use in signal-processing including radar processing [14], sequential data processing [15], audio restoration [16], image sequence restoration [17] and various other signal/image processing problems [18]–[22]. The quality of Bayesian inference across applications relies critically on the quality of the MCMC sampler employed.

Metropolis-Hastings (MH) is a popular MCMC algorithm which generates candidate iterates from a proposal distribution. The algorithm then accepts or rejects candidates with a probability calibrated to ensure the process’ stationary distribution coincides with the desired target posterior. For high-dimensional target distributions, uninformed MCMC proposals like the random-walk Metropolis struggle to efficiently explore high probability areas of the posterior. By contrast, informed gradient-based MCMC schemes utilize the local geometry of a differentiable target density to steer proposals towards areas of high probability. These strategies have proven to be quite effective. Hamiltonian Monte Carlo (HMC) [23], [24], in particular, has garnered widespread popularity for Bayesian neural networks [25], for solving complex image inverse problems [26], and for importance sampling [27], [28], to name a few research areas. Differentiability of the target density is a critical requirement for HMC and other gradient-based MCMC schemes. Bayesian models for recovering structured sparsity, however, employ non-differentiable priors by design, making it challenging to construct efficient sampling strategies.

To address this gap, [29] proposed a proximal version of the gradient-based Metropolis-adjusted Langevin algorithm (MALA) [30]. The idea is to generate proposals using a smooth approximation of a non-smooth target via the Moreau-Yosida (MY) envelope [31]. That is, proximal MCMC algorithms employ the gradient of the smooth MY-envelope in the proposal distribution, enabling the learning of local geometry despite non-smoothness. This recent success of MY-envelopes and their related proximal maps in MCMC is due to the rich literature available in convex optimization, that allows simple formulations of proximal MCMC algorithms.

In the spirit of [29], [32] proposed non-smooth HMC (ns-HMC), utilizing gradients from a smooth MY-envelope in HMC. A key reason prohibiting the wide adoption of ns-HMC is the computational cost. ns-HMC becomes computationally expensive if the proximal mapping of the log target density is not available analytically and must be computed via an iterative optimization algorithm. Whereas proximal MALA only requires two calls to the approximate gradient, ns-HMC requires multiple calls per iteration. A second drawback is that the acceptance rate of the ns-HMC algorithm is detrimentally affected by the approximation of the gradient, leading to inefficient movement in the parameter space.

Apratim Shukla and Dootika Vats are with the Department of Mathematics and Statistics, Indian Institute of Technology Kanpur, India (e-mail: apratims21@iitk.ac.in; dootika@iitk.ac.in).

Eric C. Chi is with the School of Statistics, University of Minnesota, Minneapolis, MN, USA (e-mail: echi@umn.edu).

In light of these drawbacks, we study an alternative HMC algorithm to handle non-differentiable targets – proximal HMC (p-HMC) that has been employed recently in [33] for specific use in altimetry. While p-HMC showed promise empirically, its theoretical properties remained unexplored. In this paper, we revisit p-HMC, establish key theoretical properties, and provide guidance for the selection of tuning parameters. Similar to [34], p-HMC splits the log target density into smooth and non-smooth components, and approximates only the non-smooth component by its MY-envelope. This simple difference from ns-HMC yields three key advantages.

- Closed-form MY-envelopes of many non-smooth functions are abundantly available [35] avoiding expensive iterative solvers for calculating approximate gradients.
- Since only part of the log target is approximated, the resulting gradient approximation is better, leading to improved mixing.
- It is applicable to non-convex negative log targets as long as the non-smooth component is convex. This generalizes the applicability to non-convex negative log likelihoods with sparsity inducing log-concave priors [36].

Contributions. We establish theoretical properties of the p-HMC algorithm and evaluate its effectiveness in practice. Based on our theory and experiments, we provide practical guidance on its implementation.

- We show that the proposed p-HMC algorithm converges to the target distribution ensuring the desired MCMC asymptotics.
- We provide verifiable conditions for geometric ergodicity of the p-HMC sampler. Geometric ergodicity ensures that Monte Carlo estimates of means and credible intervals have finite variance, enabling reliable simulation.
- We provide guidelines for choosing the regularization parameter in the MY-envelope threading the trade-off between smoothness and accuracy of the HMC leapfrog integrator.
- We demonstrate that p-HMC is significantly faster, easier to compute, and more effective in comparison to existing alternatives in illustrative case studies.

The remainder of the paper is organized as follows. Section II revisits the Bayesian model, reviews HMC, and surveys the literature on existing proximal MCMC methods for non-differentiable targets. Section III presents our proposed methodology. Section IV presents theoretical properties of the proposed p-HMC algorithm. Section V elaborates on the choice of an appropriate value of the regularization parameter in the MY-envelope. Section VI presents examples and demonstrates the superiority of our method over ns-HMC and other samplers. Finally, Section VII presents concluding remarks.

II. PRELIMINARIES

A. Bayesian Models

Bayesian models are often used to model signal processing data as a way to systematically incorporate prior beliefs into signal recovery [37]. Leveraging prior beliefs in this way turns poorly posed or ill-posed inverse problems into well-posed ones. For example, given an observed signal $y \in \mathbb{R}^n$, a linear

operator $B : \mathbb{R}^d \mapsto \mathbb{R}^n$, and a possibly nonlinear operator $\xi : \mathbb{R}^n \mapsto \mathbb{R}^n$, we seek to estimate the latent signal $x \in \mathbb{R}^d$ through the model

$$y = \xi(Bx). \quad (1)$$

Model (1) describes a general class of signal processing problems. For example, x may be an image that we wish to recover after corruption by a blurring filter B and some noise process described by ξ , e.g., additive noise, multiplicative noise [38], or impulsive noise models [39]. To estimate x in (1), we seek the x that minimizes some measure of discrepancy between y and $\xi(Bx)$. For instance, if ξ describes an additive Gaussian noise model and B is full rank, then the unique minimizing x is the least squares solution $\hat{x} = \arg \min_{x \in \mathbb{R}^d} \|y - Bx\|^2$; here $\|\cdot\|$ denotes Euclidean norm. However, such problems can be ill-posed, lacking uniqueness or even existence of solutions [40] when B is not full rank as is often the case in modern signal processing problems. Bayesian models provide an estimation framework that can circumvent these issues.

In Bayesian models, the latent signal x is a random variable that follows a prior distribution with density $\pi_0(x)$. Given the data y , a model or likelihood $p(y|x)$ that specifies the relationship between x and y , we seek a posterior density of x conditioned on y , denoted $\pi(x|y)$ (see [41] for more details),

$$\pi(x|y) \propto p(y|x)\pi_0(x). \quad (2)$$

The posterior can be interpreted as an update on the prior of x using the information encoded in the data y via the likelihood. Posterior distributions can be set up quite generally and include, but are not restricted to, likelihoods associated with (1). Often it is convenient to express a posterior density as

$$\pi(x) \propto \exp(-U(x)), \quad (3)$$

where $U(x) := \log \pi(x|y)$ is called the potential function. Henceforth, with a slight abuse of notation, we will denote both the target density and distribution by π . Furthermore, for notational simplicity, we denote $\pi(x|y)$ as $\pi(x)$, dropping the posterior's dependence on the data y .

An additional advantage of Bayesian methodology is that it enables rigorous statistical analysis via posterior summaries. The posterior mean and the maximum a posteriori (MAP) estimate provide point estimates of the latent signal x . Moreover, credible intervals provide quantification of posterior uncertainty in the parameters. While sampling may not be required to obtain a MAP estimate, it is indispensable for obtaining posterior means and constructing credible intervals.

MCMC algorithms provide a way to sample from (3) even when the normalizing constant is unknown. We now review MCMC basics. Let $\mathcal{B}(\mathbb{R}^d)$ be the Borel sets of \mathbb{R}^d . We generate the iterates of discrete-time time-homogeneous Markov chain $\{X_t\}_{t \geq 1}$ with a Markov transition kernel $P : \mathbb{R}^d \times \mathcal{B}(\mathbb{R}^d) \mapsto [0, 1]$. The kernel P is the conditional distribution for obtaining X_{t+1} given $X_t = x \in \mathbb{R}^d$, i.e.,

$$P(x, A) = \Pr(X_{t+1} \in A | X_t = x),$$

for all $t \geq 1$ and events A in $\mathcal{B}(\mathbb{R}^d)$. MCMC algorithms construct kernel P such that the posterior π is its stationary

distribution. If the Markov kernel P is irreducible, aperiodic, and Harris recurrent, the n -step transition kernel converges to π as $n \rightarrow \infty$, i.e.,

$$\lim_{n \rightarrow \infty} \|P^n(x, \cdot) - \pi(\cdot)\|_{\text{TV}} = 0, \quad (4)$$

where $\|\cdot\|_{\text{TV}}$ denotes the total variation distance (see [42] for definitions). The MH algorithm is a powerful method to construct such Markov kernels. The class of MH algorithms is broad and includes the random-walk Metropolis [43], MALA [30], and HMC [24]. Of these, HMC is widely acknowledged to be the most effective algorithm, particularly suited for convex potentials.

B. Hamiltonian Monte Carlo

HMC is a popular MCMC algorithm, often exhibiting superior mixing compared to other alternatives [44], [45]. We briefly overview HMC; for a more in-depth treatment, see [24].

HMC is based on the equations of motion of particles in a system [46]. At any given time t , the motion of a particle is described by its position $x \in \mathbb{R}^d$ and momentum $p \in \mathbb{R}^d$. The Hamiltonian, or total energy of the particle, is

$$H(x, p) = U(x) + K(p), \quad (5)$$

where $U(x)$ and $K(p)$ are the particle's potential and kinetic energies, respectively. The kinetic energy is defined to be $K(p) = p^\top M^{-1}p/2$, where M denotes the mass matrix of the particle. Hamilton's equations of motion govern the particle's state in the (x, p) space:

$$\frac{dp^{(i)}}{dt} = \frac{\partial H(x, p)}{\partial x^{(i)}} \quad \text{and} \quad \frac{dx^{(i)}}{dt} = -\frac{\partial H(x, p)}{\partial p^{(i)}}, \quad (6)$$

for each component $i = 1, 2, \dots, d$. If (x_t, p_t) denotes the particle's state at time t , then the equations in (6) define a Hamiltonian flow operator that takes the particle's state at time t to its state at time $t + \delta$. This is described by a mapping T_δ such that $T_\delta(x_t, p_t) = (x_{t+\delta}, p_{t+\delta})$. The solution to (6) defines the Hamiltonian path of constant energy. The movement along this path conserves the particle's total energy and describes its dynamics exactly. In the context of HMC, this is akin to sampling from the joint distribution with density,

$$\omega(x, p) \propto \exp(-U(x)) \exp\left(-\frac{p^\top M^{-1}p}{2}\right). \quad (7)$$

Marginalizing $\omega(x, p)$ over p yields density $\pi(x)$.

If we can solve (6) exactly, we can sample from $\omega(x, p)$. In practice, however, analytical solutions to (6) are rare. Therefore, (6) is numerically approximated by discretizing time at a small step size ε . A variety of symplectic integrators exist for constructing transformation mappings that approximately conserve the Hamiltonian. The most commonly used one is the leapfrog integrator, which is based on the following ε transition given a point (x_0, p_0) ,

$$p_{\frac{\varepsilon}{2}} = p_0 - \frac{\varepsilon}{2} \nabla U(x_0) \quad (8)$$

$$x_\varepsilon = x_0 + \varepsilon M^{-1} p_{\frac{\varepsilon}{2}} \quad (9)$$

$$p_\varepsilon = p_{\frac{\varepsilon}{2}} - \frac{\varepsilon}{2} \nabla U(x_\varepsilon). \quad (10)$$

The integrator, henceforth denoted by the mapping $\tilde{T}_{\varepsilon, L}$, generates a proposal value $(x_{L\varepsilon}, p_{L\varepsilon})$ by taking these three updates over L ‘‘leapfrog’’ steps. That is, $\tilde{T}_{\varepsilon, L} \approx T_{\varepsilon, L}$. The sampled point is then accepted according to the Metropolis-Hastings-Green acceptance probability,

$$\alpha(x_0, x_{L\varepsilon}) = \min \left\{ 1, e^{-H(x_{L\varepsilon}, p_{L\varepsilon}) + H(x_0, p_0)} \right\}. \quad (11)$$

Note that as $\varepsilon \rightarrow 0$, the proposed point converges to the true solution implying that $\alpha(x_0, x_{L\varepsilon}) \rightarrow 1$.

HMC and its variants [47] are common samplers employed in Bayesian signal processing as well as other Bayesian problems. Their popularity is in no small part due to their fast mixing in high-dimensions; HMC scales roughly as $O(d^{1/4})$, a significant improvement over other gradient-based schemes [44]. HMC and other gradient-based schemes, however, require $U(x)$ to be differentiable – a non-trivial inconvenience for non-differentiable target densities.

C. Proximal methods in MCMC

To apply gradient-based MCMC schemes to non-differentiable targets, we turn to proximal mappings and MY-envelopes. These building blocks enable us to infer the local geometry of non-differentiable targets without requiring differentiability.

Let $\Gamma(\mathbb{R}^d)$ denote the set of convex, lower-semicontinuous, and proper functions that map \mathbb{R}^d into $\mathbb{R} \cup \{\infty\}$.

Definition II.1. Given a positive scaling parameter λ , the Moreau-Yosida envelope of $\psi \in \Gamma(\mathbb{R}^d)$ is

$$\psi^\lambda(x) = \inf_{y \in \mathbb{R}^d} \left\{ \psi(y) + \frac{1}{2\lambda} \|y - x\|^2 \right\}. \quad (12)$$

The infimum in (12) is uniquely attained since $\psi \in \Gamma(\mathbb{R}^d)$. The minimizer of (12) defines the proximal mapping of ψ .

Definition II.2. Given a positive scaling parameter λ , the proximal mapping of $\psi \in \Gamma(\mathbb{R}^d)$ is the operator

$$\text{prox}_\psi^\lambda(x) = \arg \min_{y \in \mathbb{R}^d} \left\{ \psi(y) + \frac{1}{2\lambda} \|y - x\|^2 \right\}. \quad (13)$$

Proximal mappings are fundamental computational primitives in optimization algorithms [48]. Equation (13) can be used in (12) to evaluate the expression of ψ^λ explicitly. The MY-envelope of ψ has several useful properties: i) ψ^λ is convex whenever ψ is convex and ii) is continuously differentiable even if ψ is not [49]. The gradient of ψ^λ can be expressed in terms of the proximal mapping of ψ [35],

$$\nabla \psi^\lambda(x) = \frac{1}{\lambda} (x - \text{prox}_\psi^\lambda(x)). \quad (14)$$

Furthermore, $\nabla \psi^\lambda$ is $1/\lambda$ -Lipschitz and ψ^λ converges to ψ pointwise [49], i.e., for all $x \in \mathbb{R}^d$, $\lim_{\lambda \rightarrow 0} \psi^\lambda(x) = \psi(x)$. Thus, $\psi^\lambda(x)$ can smoothly approximate $\psi(x)$ arbitrarily well provided that λ is sufficiently small.

Proximal MCMC methods approximate non-smooth potential functions with MY-envelopes to leverage state-of-the-art gradient-based sampling schemes. Such schemes not only require differentiability but also Lipschitz differentiability to

ensure their efficiency and reliability. For example, [29] approximates a target density π with potential $U \in \Gamma(\mathbb{R}^d)$ using

$$\pi^\lambda(x) \propto \exp(-U^\lambda(x)),$$

where U^λ is the MY-envelope of U . They further employ gradients of U^λ in a MALA-like algorithm yielding proximal Metropolis-adjusted Langevin algorithm (p-MALA). Specifically, given the current state x_t , the next proposed state is

$$x^* = x_t - \frac{h}{2} \nabla U^\lambda(x_t) + \sqrt{h} \zeta, \quad (15)$$

where $\zeta \sim N(0, \mathbb{I}_d)$ and h is a step size parameter. The proposal (15) is accepted, i.e., $x_{t+1} = x^*$, according to the MH accept-reject ratio

$$\alpha(x_t, x^*) = \min \left\{ 1, \frac{\pi(x^*)q(x^*, x_t)}{\pi(x_t)q(x_t, x^*)} \right\},$$

where $q(x_t, x^*)$ is the proposal density for (15). The choice of λ in p-MALA is fixed to be $\lambda = h/2$.

MY-envelopes have also been proposed for HMC in [32], who presented the non-smooth HMC (ns-HMC). The ns-HMC employs $\nabla U^\lambda(x)$ in the leapfrog integrator of HMC, fixing $\lambda = 1$. The ns-HMC algorithm uses the following modifications to (8), (9), (10) in the standard HMC algorithm

$$p_{\frac{\varepsilon}{2}} = p_0 - \frac{\varepsilon}{2} [x_0 - \text{prox}_U^1(x_0)] \quad (16)$$

$$x_\varepsilon = x_0 + \varepsilon p_{\frac{\varepsilon}{2}} \quad (17)$$

$$p_\varepsilon = p_{\frac{\varepsilon}{2}} - \frac{\varepsilon}{2} [x_\varepsilon - \text{prox}_U^1(x_\varepsilon)], \quad (18)$$

where prox_U^1 denotes the proximal mapping of the potential U for $\lambda = 1$. The steps in (16)-(18) are repeated L times to obtain the proposed value $(x_{L\varepsilon}, p_{L\varepsilon})$. The proposal is then accepted or rejected according to (11). The ns-HMC opens the door to using HMC-like algorithms to sample from non-differentiable targets. It, however, has some drawbacks.

- The algorithm inherently assumes $\lambda = 1$ and does not explore the effect of varying λ on the performance of the algorithm.
- In Bayesian models, the likelihood is often complex enough that the proximal mapping of the full potential, U , is not available analytically. Thus, generating each proposal of ns-HMC requires L repeated calls to an iterative solver, i.e., a subroutine based on proximal splitting techniques like the forward-backward algorithm, Douglas-Rachford splitting algorithm, Dykstra-like splitting method, etc (see [48] for details). This adds a large computational burden.
- The convexity of U is a critical assumption and thus the sampler is not applicable to target densities that may not be log-concave.
- Lastly, often U is composed of a smooth and a non-smooth part. Enveloping all of U approximates both these parts leading to a cruder approximation than possibly necessary.

This last point was recognized by [34] who propose approximating only the non-smooth part of U , yielding another alternative called Moreau-Yosida MALA (my-MALA) algorithm.

Algorithm 1 p-HMC given $\varepsilon > 0$, $L \geq 1$ and $M \succ 0$

- 1) Given $X_t = x_0$, draw $p_0 \sim N(0, M)$
- 2) Use the leapfrog one- ε step equations,

$$p_{\frac{\varepsilon}{2}} = p_0 - \frac{\varepsilon}{2} \nabla U^{\lambda_g}(x_0)$$

$$x_\varepsilon = x_0 + \varepsilon M^{-1} p_{\frac{\varepsilon}{2}}$$

$$p_\varepsilon = p_{\frac{\varepsilon}{2}} - \frac{\varepsilon}{2} \nabla U^{\lambda_g}(x_\varepsilon)$$

L times sequentially to reach $(x_0, p_0) \rightarrow (x_{L\varepsilon}, p_{L\varepsilon})$

- 3) Draw $U \sim U(0, 1)$ independently, and calculate

$$\alpha(x_0, x_{L\varepsilon}) = \min \left\{ 1, e^{-H(x_{L\varepsilon}, p_{L\varepsilon}) + H(x_0, p_0)} \right\},$$

where $H(x, p) = U(x) + \frac{1}{2} p^\top M^{-1} p$ denotes total energy at (x, p)

- 4) If $U \leq \alpha(x_0, x_{L\varepsilon})$, then $X_{t+1} = x_{L\varepsilon}$
 - 5) Else $X_{t+1} = x_0$
-

III. PROXIMAL HAMILTONIAN MONTE CARLO

In this section, we adapt the methodology of [34] to address drawbacks of the ns-HMC algorithm. Let $U : \mathbb{R}^d \rightarrow \mathbb{R} \cup \{\infty\}$ be a target potential in (3) that can be expressed as

$$U(x) = f(x) + g(x),$$

where

- 1) $f : \mathbb{R}^d \rightarrow \mathbb{R}$ is a Lipschitz differentiable function with Lipschitz constant $C_f > 0$, i.e., for all $x, x' \in \mathbb{R}^d$,

$$\|\nabla f(x) - \nabla f(x')\| \leq C_f \|x - x'\|,$$

- 2) $g : \mathbb{R}^d \rightarrow \mathbb{R} \cup \{\infty\}$ is a convex, lower-semicontinuous, and proper function.

Note that f is not required to be convex unlike in [32], [34], either for the implementation or the ergodicity results of our algorithm. Thus, U may be non-convex as long as g is convex and f is Lipschitz differentiable. For our method, we propose using gradients of the following approximation:

$$U^{\lambda_g}(x) := f(x) + g^{\lambda_g}(x), \quad (19)$$

where g^{λ_g} denotes the MY-envelope of g with parameter λ_g . We propose employing a proximal HMC (p-HMC) algorithm where each leapfrog step is

$$p_{\frac{\varepsilon}{2}} = p_0 - \frac{\varepsilon}{2} \nabla U^{\lambda_g}(x_0) \quad (20)$$

$$x_\varepsilon = x_0 + \varepsilon p_{\frac{\varepsilon}{2}} \quad (21)$$

$$p_\varepsilon = p_{\frac{\varepsilon}{2}} - \frac{\varepsilon}{2} \nabla U^{\lambda_g}(x_\varepsilon). \quad (22)$$

A total of L steps are performed to get to the proposed value, that is, if $\tilde{T}_{\varepsilon, L}^{\lambda_g}$ denotes the deterministic leapfrog transition, then $\tilde{T}_{\varepsilon, L}^{\lambda_g}(x_0, p_0) = (x_{L\varepsilon}, p_{L\varepsilon})$ is the proposed value. Subsequently, this is accepted with probability,

$$\alpha(x_0, x_{L\varepsilon}) = \min \left\{ 1, e^{-H(x_{L\varepsilon}, p_{L\varepsilon}) + H(x_0, p_0)} \right\}.$$

Algorithm 1 provides pseudocode for the p-HMC sampler.

The proposed p-HMC algorithm often admits efficient implementations since proximal mappings of various g functions

are available analytically [35]. For instance, for $x \in \mathbb{R}^d$ and $\gamma, \alpha > 0$, consider the popular structure,

$$\pi(x) \propto \exp \left\{ -(\gamma \|x\|^2 + \alpha \|x\|_1) \right\}. \quad (23)$$

The proximal mapping for the ℓ_1 -norm has a closed form – the soft-thresholding operator – that can be computed in $O(d)$ flops. Thus, proposals can be generated quite cheaply since the computational cost of ∇U^{λ_g} is low. Moreover, even when a proximal mapping is available in closed form for both p-HMC and ns-HMC, our method performs better as is evidenced by the effective sample size in numerical studies (Section VI). This is because p-HMC only approximates g but takes the correct gradient contribution from f making U^{λ_g} a better approximation than U^λ . As a result, the Hamiltonian is better conserved thereby ensuring a reasonable acceptance rate. We revisit this point in more detail in Section VI.

IV. PROPERTIES OF P-HMC

We analyze the asymptotic behavior of the p-HMC algorithm. Section IV-A describes the existence of the stationary and limiting distribution of the p-HMC chain. Section IV-B details its rate of convergence.

A. Invariance and convergence

The conditions for ensuring invariance for the correct target distribution in case of HMC is more nuanced than a usual MH algorithm. This is because HMC is composed of a deterministic proposal mechanism conditioned on a randomly sampled auxiliary variable. To navigate this, we turn to the generalised version of the MH algorithm for deterministic proposals [50], the Metropolis-Hastings-Green (MHG) algorithm.

The MHG algorithm consists of augmenting the state space with that of an auxiliary variable. The auxiliary variable is then chosen randomly conditioned on the initial state of the variable of interest. Subsequently, the augmented state is then mapped to a proposal deterministically which is accepted according to the MHG ratio. More specifically, let v denote the auxiliary variable and (x, v) , the augmented space. The proposal value at any iteration $j+1$ is obtained in the following way: i) sample $v \sim q_{\text{aux}}(x_j, \cdot)$, the conditional distribution of the auxiliary variable given the previous state, and ii) employ a deterministic mapping $\phi(x_j, v) = (x^*, v^*)$ to obtain the proposed value. The resulting proposal value is then accepted with the following MHG probability,

$$\alpha(x_0, x^*) = \min \left\{ 1, \frac{\pi(x^*) q_{\text{aux}}(x^*, v^*)}{\pi(x_0) q_{\text{aux}}(x_0, v_0)} |\det J_\phi| \right\}, \quad (24)$$

where J_ϕ is the Jacobian of the mapping ϕ (see [50] for more details). In general, any algorithm employing (24) requires evaluating J_ϕ for every iteration. However, HMC avoids this due to volume preservation. Volume preservation implies that the Jacobian of transformation in the (x, p) space is unity [24]. Therefore, (24) is equivalent to accepting with probability (11).

Note that p-HMC employs the approximation ∇U^{λ_g} instead of ∇U and thus uses an approximate Hamiltonian in the proposal step. The proposal mechanism uses the leapfrog integrator, which is reversible and volume preserving. Therefore,

using the MHG accept-reject probability in (24) suffices to ensure that the samples are asymptotically from π (see [24] for a discussion). Consequently, an argument similar to [24] applies and the p-HMC algorithm is volume preserving, and thus defines a Markov kernel invariant for π .

Note that $\exp(-U^{\lambda_g}(x))$ does not need to be integrable. This eliminates the requirement of the potential U^{λ_g} to define a distribution and makes our approach broadly applicable.

B. Geometric ergodicity

The efficiency of an MCMC algorithm is typically characterized by its rate of convergence. In this respect, an important property is geometric ergodicity which we recall below.

Definition IV.1. Let P be an irreducible, aperiodic, and Harris recurrent Markov kernel with stationary distribution π . Then, for some $\rho < 1$ and $V : \mathbb{R}^d \rightarrow \mathbb{R}^+$ if,

$$\|P^n(x, \cdot) - \pi(\cdot)\|_{\text{TV}} \leq V(x)\rho^n, \quad n = 1, 2, 3, \dots \quad (25)$$

for all $x \in \mathbb{R}^d$, the Markov chain produced is said to be geometrically ergodic.

Geometric ergodicity ensures that the Markov chain explores the state space reasonably well, ensuring also the existence of a central limit theorem (CLT). Existence of a CLT is important since it enables quantifying the uncertainty in estimators of both posterior means and quantiles [51]. Under suitable conditions, the original HMC algorithm has been shown to be geometrically ergodic [45].

We next establish sufficient conditions under which our p-HMC is geometrically ergodic. Similar to the the HMC proposal, the p-HMC proposal can be written as an L -step generalisation of the proximal Langevin scheme (see [45] for details). Let x_0 be the current state and without loss of generality, $p_0 \sim N(0, M)$, where $M = \mathbb{I}_d$. The p-HMC proposal can then be expressed as

$$x_{L\varepsilon} = m_{L,\varepsilon}(x_0, p_0) + L\varepsilon p_0, \quad (26)$$

where,

$$m_{L,\varepsilon}(x_0, p_0) = x_0 - \frac{L\varepsilon^2}{2} \nabla U^{\lambda_g}(x_0) - \varepsilon^2 \sum_{i=1}^{L-1} (L-i) \nabla U^{\lambda_g}(x_{i\varepsilon}).$$

Furthermore, let the density of the proposal in (26) be denoted by $q_{\text{pH}}(x_0, x_{L\varepsilon})$ given the state x_0 . The following assumption is made to ensure that the p-HMC chain is irreducible (see [45] for details).

Assumption 1. The number of leapfrog steps L is sampled from a distribution $\mathcal{L}(\cdot)$ such that $\Pr_{\mathcal{L}}[L = 1] > 0$ and for any $(x_0, p_0) \in \mathbb{R}^{2d}$ and $\varepsilon > 0$, there is an $s < \infty$ such that $\mathbb{E}_{\mathcal{L}} [e^{s\|x_{L\varepsilon}\|}] < \infty$.

Let,

$$R(x) = \left\{ x^* : \frac{\pi(x^*) q_{\text{pH}}(x^*, x)}{\pi(x) q_{\text{pH}}(x, x^*)} < 1 \right\}$$

denote the potential rejection region and $I(x) = \{x^* : \|x^*\| \leq \|x\|\}$ denote the set of points interior to x , respectively.

Assumption 2. Let f and g be such that

- (a) $\lim_{\|x\| \rightarrow \infty} \|\nabla f(x)\| = \infty$,
- (b) $\limsup_{\|x\| \rightarrow \infty} \frac{\|\nabla f(x)\|}{\|x\|} < \infty$,
- (c) $\liminf_{\|x\| \rightarrow \infty} \frac{\langle \nabla f(x), x \rangle}{\|\nabla f(x)\| \|x\|} > 0$, and
- (d) $\lim_{\|x\| \rightarrow \infty} \frac{\|\nabla g^{\lambda_g}(x)\|}{\|\nabla f(x)\|} < 1$.

Theorem 1. Under Assumptions 1 and 2, a p-HMC ergodic Markov chain is geometrically ergodic if,

$$\lim_{\|x\| \rightarrow \infty} \int_{R(x) \cap I(x)} q_{\text{pH}}(x, x^*) dx^* = 0. \quad (27)$$

Proof. See Appendix A-A. \square

Remark 1. Condition (a) of Assumption 2 ensures that the target density function $\pi(x)$ decays in the tails whereas condition (b) states that the rate of growth in $\nabla f(x)$ is asymptotically sublinear. Condition (c) is the ‘inwards convergence’ condition (see [45]). Condition (d) relates to the specific form of penalty function g^{λ_g} compared to f . It implies that the rate of growth of ∇g^{λ_g} is not faster than that of ∇f . This can occur naturally as we describe next.

C. Example: The ℓ_1 -norm prior

Consider $g(x) = \|x\|_1 = \|(x_{(1)}, \dots, x_{(d)})^\top\|$. This is the popular ℓ_1 -penalty which is common in many Bayesian problems [52], [53]. Here,

$$[\text{prox}_g^{\lambda_g}(x)]_i = \begin{cases} x_{(i)} - \lambda_g & \text{if } x_{(i)} > \lambda_g \\ x_{(i)} + \lambda_g & \text{if } x_{(i)} < -\lambda_g \\ 0 & \text{if } |x_{(i)}| \leq \lambda_g \end{cases} \quad i = 1, 2, \dots, d, \quad (28)$$

which is the element-wise soft-thresholding operator. Therefore,

$$[\nabla g^{\lambda_g}(x)]_i = \begin{cases} 1 & \text{if } x_{(i)} > \lambda_g \\ -1 & \text{if } x_{(i)} < -\lambda_g \\ x_{(i)}/\lambda_g & \text{if } |x_{(i)}| \leq \lambda_g. \end{cases} \quad (29)$$

This implies, under Assumption 2(a) that

$$\frac{\|\nabla g^{\lambda_g}(x)\|}{\|\nabla f(x)\|} \leq \frac{\sqrt{d}}{\|\nabla f(x)\|} \rightarrow 0 \quad \text{as} \quad \|x\| \rightarrow \infty.$$

Thus, condition (d) holds for the ℓ_1 -norm provided (a) holds.

V. CHOICE OF λ_g

The choice of the regularisation parameter is critical to the performance of any proximal MCMC algorithm. Whereas [32] fix $\lambda = 1$ for ns-HMC, such a choice may not be universally suitable over all applications and datasets. Indeed, λ_g 's value trades-off smoothness of U^{λ_g} and its quality of approximation to the target Hamiltonian. That is, increasing the penalty makes the potential smoother, but reduces the acceptance probability since the true Hamiltonian is less preserved. This trade-off must be balanced for effective sampling. In this section, we provide guidance on choosing λ_g .

Intuitively, we should choose λ_g so that the approximation error in g^{λ_g} is small compared to the information in f about

U . For instances where f contributes more information to U , a larger discrepancy between g and g^{λ_g} might be tolerable, but for instances where f contributes less to U compared to g , the approximation error in g^{λ_g} must be restricted. With this in mind, let x_0 be a minimizer of U so that $0 \in \partial U(x_0)$, where ∂U denotes the subdifferential of U . Note that x_0 is not a minimizer of U^{λ_g} although x_0 will be close to a minimizer of U^{λ_g} for a small enough λ_g .

Let $L = 1$ and (x_0, p_0) be the initial point. Consider $\varepsilon \approx 0$ so that the approximation error to the Hamiltonian is dominated by the MY-smoothing. We track the relative change in the Hamiltonian H for one leapfrog step over a range of λ_g . For sufficiently large λ_g , the approximation error in using g^{λ_g} will be large enough to detrimentally impact the approximation to the Hamiltonian. Thus, consider the metric

$$R^{\lambda_g} = \left| \frac{H(x_0, p_0) - H\left(\tilde{T}_{\varepsilon, L}^{\lambda_g}(x_0, p_0)\right)}{H(x_0, p_0)} \right|. \quad (30)$$

Equation (30) measures the relative difference in the value of the Hamiltonians of the target at the initial and the proposed point, respectively. Recall that for $\varepsilon \approx 0$, $U^{\lambda_g}(x) \rightarrow U(x)$ for all x as $\lambda_g \rightarrow 0$ and consequently $H\left(\tilde{T}_{\varepsilon, L}^{\lambda_g}(x_0, p_0)\right)$ tends to $H(x_0, p_0)$ as $\lambda_g \rightarrow 0$. Thus, on the one hand, with $\varepsilon \approx 0$, the relative error R^{λ_g} becomes very small as $\lambda_g \rightarrow 0$, ensuring high acceptance rates of the algorithm. On the other hand, increasing λ_g smooths the potential yielding better behaved gradients. There is thus, a trade-off between choosing a large λ_g , which ensures smoothness in the approximated potential, and a small one, which increases the acceptance rate.

Figure 1 shows how R^{λ_g} varies with λ_g for the three examples in Section VI. In all three examples, R^{λ_g} is nondecreasing in λ_g . We recommend choosing the largest λ_g so that R^{λ_g} remains small.

VI. NUMERICAL STUDIES

This section demonstrates the usefulness of the p-HMC algorithm over ns-HMC and other MCMC methods. We begin with a one dimensional Bayesian lasso example which provides some validation for the proposed choice of λ_g in the p-HMC algorithm. The next two examples, are low-dimensional signal recovery problems which illustrate the advantages of p-HMC over the alternatives in terms of mixing and estimation accuracy. We use $M = \mathbb{I}_d$ for all the implementations. The code is available at <https://github.com/sapratim/P-HMC>.

A. Toy example

We first consider a simple one-dimensional problem where we compare the leapfrog discretization for both p-HMC and ns-HMC. We use this simple case study to visualize the effects of λ_g (p-HMC) and λ (ns-HMC) on the numerical integrator and the subsequent leapfrog trajectories' deviation from the true potential.

For $n = 100$, let $y = (y_1, y_2, \dots, y_n)$ and for $x \in \mathbb{R}$, consider the target density with potential

$$U(x) = \frac{1}{2} \sum_{i=1}^n (y_i - x)^2 + |x| =: f(x) + g(x). \quad (31)$$

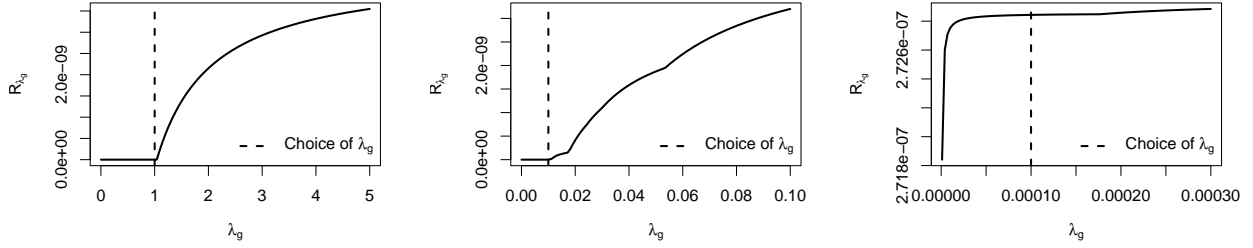


Fig. 1: Choice of λ_g for the three examples in Section VI, with $\varepsilon = 10^{-7}$: (left) Toy example, (middle) sparse logistic regression, (right) low-rank matrix estimation.

For this one-dimensional Bayesian lasso-like model in (31), we draw contours of $e^{-H(x,p)}$ to visualize how well the leapfrog steps of each algorithm hug the contour. The proximal mappings of g and U are available in closed form:

$$\text{prox}_g^{\lambda_g}(x) = \text{sign}(x) \cdot \max\{|x| - \lambda_g, 0\} \quad \text{and}, \quad (32)$$

$$\text{prox}_U^{\lambda}(x) = \text{sign}(w) \cdot \max\left\{|w| - \frac{\lambda}{1+n\lambda}, 0\right\}, \quad (33)$$

where $w = (x + \lambda \sum_i y_i)/(1 + n\lambda)$. We generate $y_i \stackrel{\text{iid}}{\sim} N(1, 0.5)$. Using the proximal mappings in (32) and (33), for fixed $\lambda_g, \lambda, \varepsilon$, and L , we plot the leapfrog steps of the integrators for p-HMC and ns-HMC. Figure 2 shows that the leapfrog steps generated by p-HMC hug the Hamiltonian contour well for an extremely wide range of λ_g choices, whereas the leapfrog steps generated by ns-HMC are not as reliable. Specifically, ns-HMC's steps can hug the contour closely for $\lambda = 0.001$ but may go far off course for larger λ . p-HMC's ability to conserve the Hamiltonian with high fidelity across a wide range of λ_g ensures high acceptance rates and quality of sampling that is fairly agnostic to the choice of λ_g .

B. Sparse logistic regression

We next consider the popular sparse logistic regression model. The data consists of n binary responses, i.e., $y = (y_1, \dots, y_n)$ where each y_i is zero or one, and predictor variables $x_i \in \mathbb{R}^d$ for $i = 1, \dots, n$. We assume the y_i 's are independent and $y_i = 1$ with probability $(1 + \exp(-x_i^T \beta))^{-1}$, where $\beta \in \mathbb{R}^d$ is a regression parameter of interest. To recover a sparse model, we assume an ℓ_1 -prior on β . This acts as the non-differentiable component in the posterior distribution with proximal mapping given as the elementwise soft-thresholding operator (28). Proximal mapping for the full potential is not analytically available, making ns-HMC expensive to implement. Further details are provided in Appendix A-B.

We use the `Pima.tr` dataset available in library `MASS` in R. It contains 200 randomly selected diabetic females in Phoenix, Arizona, from a total of 532 patients collected by US National Institute of Diabetes and Digestive and Kidney Diseases [54]. It has 7 covariates and a binary response vector encoding whether diabetes was tested positive or negative.

We implement ns-HMC with $\lambda = 1$ and p-HMC with $\lambda_g = 0.01$ (see middle panel of Figure 1) respectively, and run both chains for $N = 10^5$ iterations. We fix $L = 10$ for both ns-HMC and p-HMC, with $\varepsilon = 0.00014$ for ns-HMC and $\varepsilon = 0.00192$ for p-HMC. Figure 3 compares the autocorrelation functions of both chains, demonstrating the improved performance of the p-HMC sampler. For additional comparisons, we run a random walk Metropolis with a Gaussian proposal (RWM), the p-MALA of [29], and the my-MALA of [34]. Each Markov chain was run for $N = 10^5$ iterations starting from the MAP. To further compare the performance, we repeat the simulations 100 times and report the median, minimum, and maximum effective sample size (ESS) per second averaged over the replications of all the components. Table I reports these ESS comparisons. Note that ns-HMC has the lowest ESS per second among all algorithms across all variables and p-HMC outperforms it significantly.

Method	min	median	max
RWM	4.819	95.063	503.129
p-HMC	3.239	454.372	3556.195
my-MALA	2.199	22.598	128.345
ns-HMC	0.002	0.013	0.065
p-MALA	0.113	0.922	4.661

TABLE I: Minimum, median, and maximum ESS per second for all components, averaged over 100 replications.

C. Nuclear-norm based low-rank matrix estimation

Low-rank matrix estimation is an important problem in matrix recovery problems, e.g., matrix completion and image denoising. The nuclear norm prior has enjoyed widespread use in these problems [55]–[58].

We observe a matrix $Y \in \mathbb{R}^{m \times k}$ where $Y = X + E$. We wish to recover the latent low-rank matrix X that has been corrupted by a noise matrix E with iid Gaussian entries, i.e., $e_{ij} \stackrel{\text{iid}}{\sim} N(0, \sigma^2)$, where $\sigma^2 > 0$ is known. The assumed prior on X is,

$$\pi_0(X) \propto \exp(-\alpha \|X\|_*), \quad (34)$$

where $\|X\|_*$ is the nuclear norm of X and $\alpha > 0$ is constant. Recall that $\|X\|_*$ is the sum of the singular values of X . The

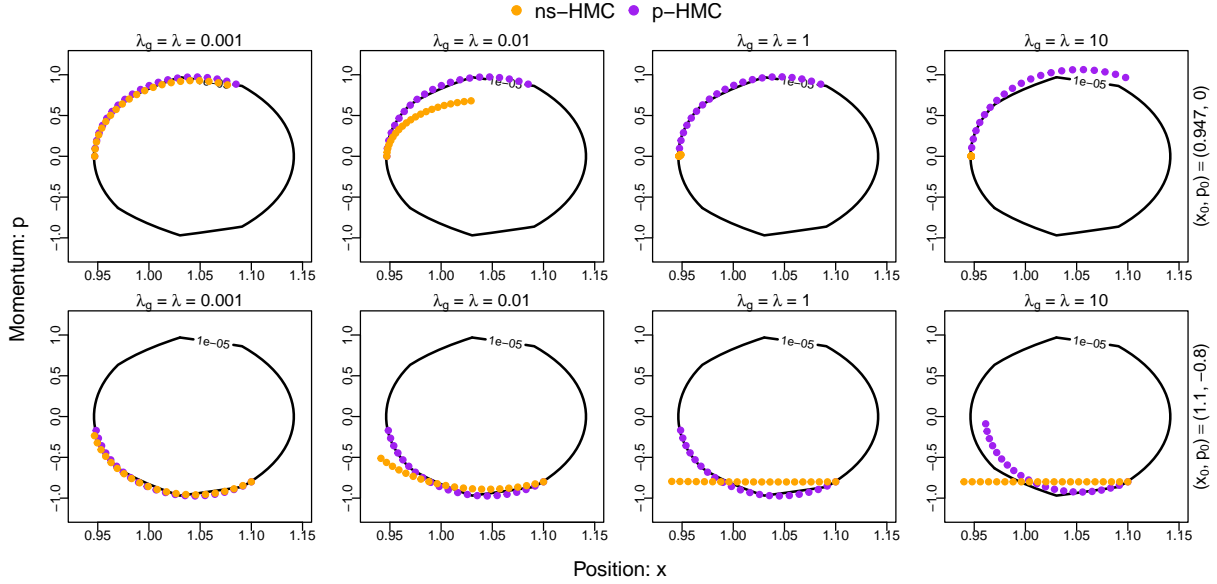


Fig. 2: Toy example: Leapfrog discretised step for $\varepsilon = 0.01$ and $L = 20$ with two different starting values in each row.

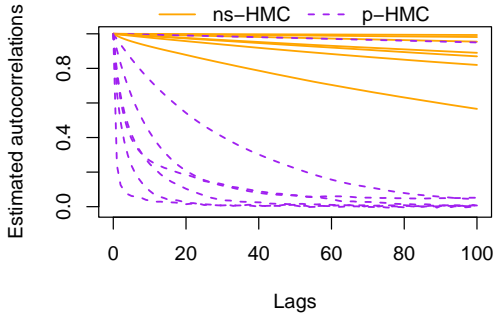


Fig. 3: Estimated autocorrelation functions for ns-HMC and p-HMC for all marginal components.

posterior density of X given Y is

$$\pi(X|Y) \propto \exp \left\{ - \left(\frac{\|Y - X\|_F^2}{2\sigma^2} + \alpha \|X\|_* \right) \right\}, \quad (35)$$

where $\|X\|_F$ denotes the Frobenius norm of X . We split the potential in (35) as the sum of $f(X) := \|Y - X\|_F^2 / 2\sigma^2$ and $g(X) := \alpha \|X\|_*$. For p-HMC, the proximal mapping of g is given by,

$$\text{prox}_g^{\lambda g}(X) = \text{SVT}(X, \alpha\lambda g)$$

where $\text{SVT}(X, \tau)$ denotes the singular value soft-thresholding operator on matrix X with threshold τ . Let $X = B\Sigma_\tau D^\top$, where Σ_τ is the diagonal matrix of singular values and let s_i denote the i^{th} corresponding singular value. Then $\text{SVT}(X, \tau) = B\Sigma_\tau D^\top$ where Σ_τ denotes the matrix obtained by replacing each singular value s_i by $\max(s_i - \tau, 0)$. Similarly for ns-HMC, the proximal mapping for $U = f + g$ is [59],

$$\text{prox}_U^\lambda(X) = \text{SVT} \left(\frac{\lambda}{\lambda + \sigma^2} Y + \frac{\sigma^2}{\lambda + \sigma^2} X, \frac{\alpha\lambda\sigma^2}{\lambda + \sigma^2} \right).$$

We use a 64×64 pixel checkerboard image similar to the one in [29] for our analysis. The dimension of the posterior distribution is $64^2 (= 4096)$ with $\sigma^2 = 0.01$ and $\alpha = 1.15/\sigma^2$ as chosen in [29]. Following the guidance given in Section V, we choose $\lambda_g = 0.0001$. As in prior examples, we run ns-HMC with $\lambda = 1$ and run the chains for a total of $N = 10^5$ iterations. Table II compares the ESS of ns-HMC and p-HMC with that of RWM, p-MALA and my-MALA. We see that p-HMC has the highest ESS per second for all the minimum, median and the maximum variable as described below. Evidence for p-HMC's better mixing is corroborated by the autocorrelation plots in Figure 4 which shows the gains in mixing of p-HMC over ns-HMC for all the components.

Figure 5 describes variants of the checkerboard image considered for this problem. The first three images display the latent matrix X , observed matrix Y and the denoised MAP estimate respectively. The last image visualizes the uncertainty in the estimated pixels. For each pixel a credible interval is constructed. The pixels having the widest intervals (95th percentile) are plotted in white, allowing an assessment of which pixels demonstrate larger posterior uncertainty.

Method	min	median	max
RWM	0.169	0.217	1.406
pHMC	10.545	11.500	12.798
myMALA	0.696	0.791	0.907
nsHMC	0.004	0.005	0.007
pMALA	0.640	0.726	0.829

TABLE II: Minimum, median, and maximum ESS per second for all components, averaged over 100 replications.

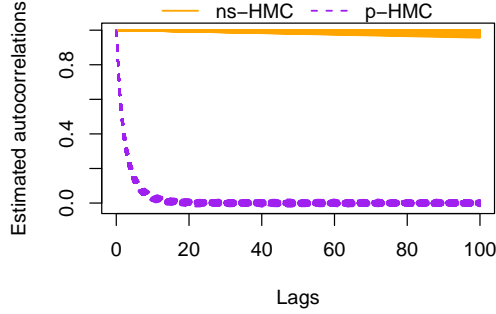


Fig. 4: Nuclear Norm: Estimated autocorrelation functions for ns-HMC and p-HMC for all marginal components.

VII. CONCLUSION

This work explores an efficient proximal HMC method for non-smooth targets. It is useful for non-differentiable target densities, which are ubiquitous in signal/image processing. Leveraging the properties of proximal mappings, the described methodology achieves significant computational gains. In cases where the computational cost between the proposed p-HMC method and ns-HMC is the same, our method achieves significantly more accurate results as measured by the effective sample size. This is demonstrated in the examples where our method successfully outperforms in either the computational cost or the estimation accuracy. We also present novel theoretical analysis for p-HMC. Specifically, we provide verifiable conditions for geometric ergodicity of the p-HMC chain. Finally, we provide practical guidance on choosing the smoothing parameter λ that tunes the degree of approximation to the target potential.

APPENDIX A

A. Proof of Theorem 1

We first state useful results from [45].

Theorem 2 ([45]). An HMC algorithm produces a π -geometrically ergodic Markov chain if i) Assumption 1 holds and ii) for $1/2 < \delta < 1$,

$$\limsup_{\|x\| \rightarrow \infty, \|z\| \leq \|x\|^\delta} \{\|m_{L,\varepsilon}(x, z)\| - \|x\|\} < -\sqrt{2}L\varepsilon\eta(d), \quad (36)$$

where $\eta(d) = \Gamma((d+1)/2)/\Gamma(d/2)$, and iii)

$$\lim_{\|x\| \rightarrow \infty} \int_{R(x) \cap I(x)} q_H(x, y) dy = 0. \quad (37)$$

Condition (36) is challenging to verify in practice, so [45] provide the following sufficient condition that we use to prove Theorem 1.

Theorem 3 ([45]). For any $L \geq 1$, (36) holds if

$$(a) \quad \lim_{\|x\| \rightarrow \infty} \|\nabla U(x)\| = \infty, \quad (38)$$

$$(b) \quad \liminf_{\|x\| \rightarrow \infty} \frac{\langle \nabla U(x), x \rangle}{\|\nabla U(x)\| \|x\|} > 0, \quad (39)$$

$$(c) \quad \limsup_{\|x\| \rightarrow \infty} \frac{\|\nabla U(x)\|}{\|x\|} = S_l, \quad (40)$$

for some $S_l < \infty$, then there exists an $\varepsilon_0 < \infty$ such that (36) holds provided $\varepsilon < \varepsilon_0$.

Proof of Theorem 1. It suffices to prove that (38), (39) and (40) hold under Assumption 2. We first verify (38). By parts (a) and (b) of Assumption 2

$$\begin{aligned} \lim_{\|x\| \rightarrow \infty} \|\nabla U^{\lambda g}(x)\| &= \lim_{\|x\| \rightarrow \infty} \|\nabla f(x) + \nabla g^{\lambda g}(x)\| \\ &\geq \lim_{\|x\| \rightarrow \infty} \|\nabla f(x)\| - \lim_{\|x\| \rightarrow \infty} \|g^{\lambda g}(x)\| \\ &= \lim_{\|x\| \rightarrow \infty} \|\nabla f(x)\| \left(1 - \frac{\|\nabla g^{\lambda g}(x)\|}{\|\nabla f(x)\|}\right) \\ &\rightarrow \infty. \end{aligned}$$

We next verify (39). Note that

$$\begin{aligned} \liminf_{\|x\| \rightarrow \infty} \frac{\langle \nabla U^{\lambda g}(x), x \rangle}{\|\nabla U^{\lambda g}(x)\| \|x\|} \\ \geq \liminf_{\|x\| \rightarrow \infty} \frac{\langle \nabla f(x), x \rangle}{\|\nabla U^{\lambda g}(x)\| \|x\|} + \liminf_{\|x\| \rightarrow \infty} \frac{\langle \nabla g^{\lambda g}(x), x \rangle}{\|\nabla U^{\lambda g}(x)\| \|x\|}. \end{aligned} \quad (41)$$

We derive bounds on the two terms on the right hand side of the inequality in (41). We first show that

$$\liminf_{\|x\| \rightarrow \infty} \frac{\langle \nabla g^{\lambda g}(x), x \rangle}{\|\nabla U^{\lambda g}(x)\| \|x\|} \geq 0. \quad (42)$$

Since g is convex, its MY-envelope $g^{\lambda g}$ is also convex. Recall that the gradient of a differentiable convex function is monotone, i.e., for any x and y in \mathbb{R}^d ,

$$\langle \nabla g^{\lambda g}(x) - \nabla g^{\lambda g}(y), x - y \rangle \geq 0. \quad (43)$$

Taking $y = 0$ in (43) gives

$$\langle \nabla g^{\lambda g}(x), x \rangle \geq \langle \nabla g^{\lambda g}(0), x \rangle.$$

Therefore,

$$\liminf_{\|x\| \rightarrow \infty} \frac{\langle \nabla g^{\lambda g}(x), x \rangle}{\|\nabla U^{\lambda g}(x)\| \|x\|} \geq \liminf_{\|x\| \rightarrow \infty} \frac{\langle \nabla g^{\lambda g}(0), x \rangle}{\|\nabla U^{\lambda g}(x)\| \|x\|} \quad (44)$$

$$\geq - \liminf_{\|x\| \rightarrow \infty} \frac{\|\nabla g^{\lambda g}(0)\| \|x\|}{\|\nabla U^{\lambda g}(x)\| \|x\|} \quad (45)$$

$$= 0. \quad (46)$$

Now we turn our attention to bounding the second term in (41). Note that

$$\begin{aligned} \liminf_{\|x\| \rightarrow \infty} \frac{\langle \nabla f(x), x \rangle}{\|\nabla U^{\lambda g}(x)\| \|x\|} &= \liminf_{\|x\| \rightarrow \infty} \frac{\langle \nabla f(x), x \rangle}{\|\nabla f(x) + \nabla g^{\lambda g}(x)\| \|x\|} \\ &\geq \liminf_{\|x\| \rightarrow \infty} \left(\frac{1}{(1 + \|\nabla g^{\lambda g}(x)\|/\|\nabla f(x)\|)} \cdot \frac{\langle \nabla f(x), x \rangle}{\|\nabla f(x)\| \|x\|} \right). \end{aligned}$$

By parts (b) and (c) of Assumption 2, the right hand side of the inequality in (44) is strictly positive which together with (42) establishes (39).

Finally, we verify (40). By parts (b) and (d) of Assump-

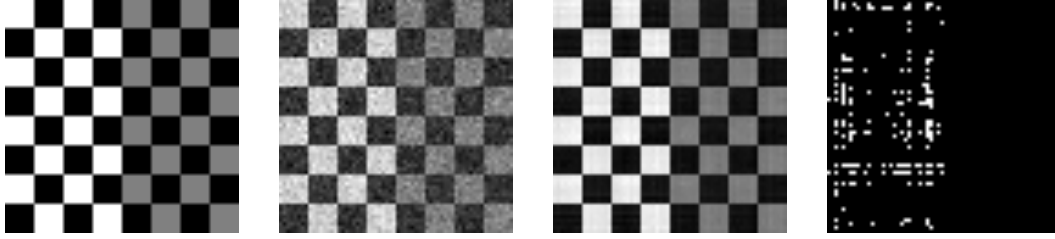


Fig. 5: (From left) Original matrix, noisy matrix, MAP estimator, top 5% elements with the largest credible intervals, in white.

tion 2,

$$\begin{aligned}
\frac{\|\nabla U^{\lambda g}(x)\|}{\|x\|} &\leq \frac{\|\nabla f(x)\|}{\|x\|} + \frac{\|\nabla g^{\lambda g}(x)\|}{\|x\|} \\
\Rightarrow \limsup_{\|x\| \rightarrow \infty} \frac{\|\nabla U^{\lambda g}(x)\|}{\|x\|} & \\
&\leq \limsup_{\|x\| \rightarrow \infty} \frac{\|\nabla f(x)\|}{\|x\|} + \limsup_{\|x\| \rightarrow \infty} \frac{\|\nabla g^{\lambda g}(x)\| \|\nabla f(x)\|}{\|\nabla f(x)\| \|x\|} \\
&\leq \limsup_{\|x\| \rightarrow \infty} \frac{\|\nabla f(x)\|}{\|x\|} \\
&\quad + \lim_{\|x\| \rightarrow \infty} \frac{\|\nabla g^{\lambda g}(x)\|}{\|\nabla f(x)\|} \cdot \limsup_{\|x\| \rightarrow \infty} \frac{\|\nabla f(x)\|}{\|x\|} \\
&= \left(1 + \lim_{\|x\| \rightarrow \infty} \frac{\|\nabla g^{\lambda g}(x)\|}{\|\nabla f(x)\|}\right) \limsup_{\|x\| \rightarrow \infty} \frac{\|\nabla f(x)\|}{\|x\|} \\
&< \infty.
\end{aligned}$$

Consequently, by Theorem 3 the p-HMC algorithm is geometrically ergodic under Assumptions 1 and 2. \square

B. Details of Section VI-B

We derive the expression of the posterior density for the sparse logistic regression example and also provide details on employing ns-HMC. Let $\pi_0(\beta)$ denote the prior on β

$$\pi_0(\beta) = \prod_{j=1}^d \frac{\alpha \exp(-\alpha|\beta_j|)}{2}, \quad \beta \in \mathbb{R}^d. \quad (47)$$

The resulting posterior density is

$$\begin{aligned}
\pi(\beta|y) &\propto \exp\left(-\left(\sum_{i=1}^n \log(1 + e^{x_i^\top \beta}) - y_i x_i^\top \beta + \alpha \|\beta\|_1\right)\right) \\
&= \exp(-U(\beta)).
\end{aligned}$$

Define $U(\beta) = f(\beta) + g(\beta)$ where

$$f(\beta) = \sum_{i=1}^n \log(1 + e^{x_i^\top \beta}) - y_i x_i^\top \beta \quad \text{and} \quad g(\beta) = \alpha \|\beta\|_1.$$

Recall

$$\nabla g^{\lambda g}(\beta) = \frac{\beta - \text{prox}_g^{\lambda g}(\beta)}{\lambda},$$

where $\text{prox}_g^{\lambda g}$ is the soft-thresholding operator. We compare our approach to ns-HMC method [32] which requires the

proximal mapping of U^λ

$$\text{prox}_U^\lambda(\beta) = \arg \min_{z \in \mathbb{R}^d} \left\{ \sum_{i=1}^n \left(\log(1 + e^{x_i^\top z}) - y_i x_i^\top z \right) + \alpha \|z\|_1 + \frac{1}{2\lambda} \|\beta - z\|^2 \right\}.$$

This does not have a closed form expression and requires an iterative solver. We employ the FISTA solver [60].

REFERENCES

- [1] D. Manolakis, V. Ingle, and S. Kogon, *Statistical and Adaptive Signal Processing: Spectral Estimation, Signal Modeling, Adaptive Filtering, and Array Processing*. Artech House signal processing library, Artech House, 2005.
- [2] D. L. Donoho, "Compressed sensing," *IEEE Trans. Inform. Theory*, vol. 52, no. 4, pp. 1289–1306, 2006.
- [3] D. L. Donoho and I. M. Johnstone, "Adapting to unknown smoothness via wavelet shrinkage," *J. Amer. Statist. Assoc.*, vol. 90, no. 432, pp. 1200–1224, 1995.
- [4] D. L. Donoho and I. M. Johnstone, "Ideal spatial adaptation by wavelet shrinkage," *Biometrika*, vol. 81, no. 3, pp. 425–455, 1994.
- [5] F. Costa, H. Batatia, L. Chaari, and J.-Y. Tournet, "Sparse EEG source localization using Bernoulli Laplacian priors," *IEEE Transactions on Biomedical Engineering*, vol. 62, no. 12, pp. 2888–2898, 2015.
- [6] M. Lebrun, A. Buades, and J. M. Morel, "A nonlocal Bayesian image denoising algorithm," *SIAM Journal on Imaging Sciences*, vol. 6, no. 3, pp. 1665–1688, 2013.
- [7] C. Chau, P. L. Combettes, J.-C. Pesquet, and V. R. Wajs, "Iterative image deconvolution using overcomplete representations," in *2006 14th European Signal Processing Conference*, pp. 1–5, IEEE, 2006.
- [8] S. C. Park, M. K. Park, and M. G. Kang, "Super-resolution image reconstruction: A technical overview," *IEEE signal processing magazine*, vol. 20, no. 3, pp. 21–36, 2003.
- [9] V. I. Morgenshtern and E. J. Candès, "Super-resolution of positive sources: The discrete setup," *SIAM Journal on Imaging Sciences*, vol. 9, no. 1, pp. 412–444, 2016.
- [10] M. Lustig, D. Donoho, and J. M. Pauly, "Sparse MRI: The application of compressed sensing for rapid MR imaging," *Magnetic Resonance in Medicine: An Official Journal of the International Society for Magnetic Resonance in Medicine*, vol. 58, no. 6, pp. 1182–1195, 2007.
- [11] Z. Khan, T. Balch, and F. Dellaert, "An MCMC-based particle filter for tracking multiple interacting targets," in *Computer Vision - ECCV 2004* (T. Pajdla and J. Matas, eds.), (Berlin, Heidelberg), pp. 279–290, Springer Berlin Heidelberg, 2004.
- [12] J. Spall, "Estimation via Markov chain Monte Carlo," *IEEE Control Systems Magazine*, vol. 23, no. 2, pp. 34–45, 2003.
- [13] C. P. Robert and G. Casella, *Monte Carlo Statistical Methods*. Springer Texts in Statistics, Springer-Verlag, New York, second ed., 2004.
- [14] J. L. Noga and W. J. Fitzgerald, "Modelling sea clutter using conditional heteroscedastic models," in *9th European Signal Processing Conference (EUSIPCO 1998)*, pp. 1–4, 1998.
- [15] A. Brockwell, P. Del Moral, and A. Doucet, "Sequentially interacting Markov chain Monte Carlo methods," *The Annals of Statistics*, vol. 38, no. 6, pp. 3387–3411, 2010.

- [16] J. 6 Ruanaidh and W. Fitzgerald, "Interpolation of missing samples for audio restoration," *Electronics Letters*, vol. 30, no. 8, pp. 622–623, 1994.
- [17] R. Morris, W. Fitzgerald, and A. Kokaram, "A sampling based approach to line scratch removal from motion picture frames," in *Proceedings of 3rd IEEE International Conference on Image Processing*, vol. 1, pp. 801–804 vol.1, 1996.
- [18] W. Fitzgerald, "Markov chain Monte Carlo methods with applications to signal processing," *Signal Processing*, vol. 81, no. 1, pp. 3–18, 2001. Special section on Markov Chain Monte Carlo (MCMC) Methods for Signal Processing.
- [19] A. Doucet and X. Wang, "Monte Carlo methods for signal processing: A review in the statistical signal processing context," *IEEE Signal Processing Magazine*, vol. 22, no. 6, pp. 152–170, 2005.
- [20] Y. Marnissi, A. Benazza-Benyahia, E. Chouzenoux, and J.-C. Pesquet, "Majorize-minimize adapted Metropolis-Hastings algorithm. Application to multichannel image recovery," in *2014 22nd European Signal Processing Conference (EUSIPCO)*, pp. 1332–1336, 2014.
- [21] C. Gilavert, S. Moussaoui, and J. Idier, "Efficient Gaussian sampling for solving large-scale inverse problems using MCMC," *IEEE Transactions on Signal Processing*, vol. 63, no. 1, pp. 70–80, 2015.
- [22] D. Luengo, L. Martino, M. Bugallo, V. Elvira, and S. Särkkä, "A survey of Monte Carlo methods for parameter estimation," *EURASIP Journal on Advances in Signal Processing*, vol. 2020, no. 1, p. 25, 2020.
- [23] K. M. Hanson, "Markov chain Monte Carlo posterior sampling with the Hamiltonian method," in *Medical Imaging 2001: Image Processing*, vol. 4322, pp. 456–467, SPIE, 2001.
- [24] R. M. Neal *et al.*, "MCMC using Hamiltonian dynamics," *Handbook of Markov chain Monte Carlo*, vol. 2, no. 11, p. 2, 2011.
- [25] P. Izmailov, S. Vikram, M. D. Hoffman, and A. G. G. Wilson, "What are Bayesian neural network posteriors really like?," in *International Conference on Machine Learning*, pp. 4629–4640, PMLR, 2021.
- [26] Y. Altmann, N. Dobigeon, and J.-Y. Tourneret, "Unsupervised post-nonlinear unmixing of hyperspectral images using a Hamiltonian Monte Carlo algorithm," *IEEE Transactions on Image Processing*, vol. 23, no. 6, pp. 2663–2675, 2014.
- [27] A. Mousavi, R. Monsefi, and V. Elvira, "Hamiltonian adaptive importance sampling," *IEEE Signal Processing Letters*, vol. 28, pp. 713–717, 2021.
- [28] F. Llorente, E. Curbelo, L. Martino, V. Elvira, and D. Delgado, "MCMC-driven importance samplers," *Applied Mathematical Modelling*, vol. 111, pp. 310–331, 2022.
- [29] M. Pereyra, "Proximal Markov chain Monte Carlo Algorithms," *Statistics and Computing*, vol. 26, pp. 745–760, 2016.
- [30] G. O. Roberts and R. L. Tweedie, "Exponential convergence of Langevin distributions and their discrete approximations," *Bernoulli*, pp. 341–363, 1996.
- [31] J.-J. Moreau, "Fonctions convexes duales et points proximaux dans un espace hilbertien," *C. R. Acad. Sci. Paris*, vol. 255, pp. 2897–2899, 1962.
- [32] L. Chaari, J.-Y. Tourneret, C. Chaux, and H. Batatia, "A Hamiltonian Monte Carlo method for non-smooth energy sampling," *IEEE Transactions on Signal Processing*, vol. 64, no. 21, pp. 5585–5594, 2016.
- [33] M. Guo, B. Huang, L. Yang, and G. Jiang, "Above ground level estimation for radar altimetry using proximal Hamiltonian Monte Carlo," *IEEE Journal on Miniaturization for Air and Space Systems*, vol. 5, no. 3, pp. 128–137, 2023.
- [34] A. Durmus, É. Moulines, and M. Pereyra, "A Proximal Markov chain Monte Carlo method for Bayesian inference in imaging inverse problems: When Langevin meets Moreau," *SIAM Review*, vol. 64, no. 4, pp. 991–1028, 2022.
- [35] N. Parikh, S. Boyd, *et al.*, "Proximal Algorithms," *Foundations and trends® in Optimization*, vol. 1, no. 3, pp. 127–239, 2014.
- [36] W. Wright, "Bayesian approach to neural-network modeling with input uncertainty," *IEEE Transactions on Neural Networks*, vol. 10, no. 6, pp. 1261–1270, 1999.
- [37] J. V. Candy, *Bayesian signal processing*. Wiley Series on Adaptive and Cognitive Dynamic Systems, John Wiley & Sons, Inc., Hoboken, NJ, second ed., 2016. Classical, modern, and particle filtering methods.
- [38] G. Aubert and J.-F. Aujol, "A variational approach to removing multiplicative noise," *SIAM journal on applied mathematics*, vol. 68, no. 4, pp. 925–946, 2008.
- [39] J.-F. Cai, R. H. Chan, and M. Nikolova, "Fast two-phase image deblurring under impulse noise," *Journal of Mathematical Imaging and Vision*, vol. 36, no. 1, pp. 46–53, 2010.
- [40] Y. Marnissi, *Bayesian methods for inverse problems in signal and image processing*. PhD thesis, Université Paris-Est, 2017.
- [41] C. P. Robert, *The Bayesian choice*. Springer Texts in Statistics, Springer, New York, second ed., 2007. From decision-theoretic foundations to computational implementation.
- [42] S. P. Meyn and R. L. Tweedie, *Markov Chains and Stochastic Stability*. Cambridge University Press, 2009.
- [43] N. Metropolis, A. W. Rosenbluth, M. N. Rosenbluth, A. H. Teller, and E. Teller, "Equations of state calculations by Fast Computing Machine," *Journal of Chemical Physics*, vol. 21, 1953.
- [44] A. Beskos, N. S. Pillai, G. O. Roberts, J. Sanz-Serna, and A. Stuart, "Optimal tuning of the hybrid Monte Carlo algorithm," *Bernoulli*, vol. 19, no. 5a, pp. 1501–1534, 2013.
- [45] S. Livingstone, M. Betancourt, S. Byrne, and M. Girolami, "On the geometric ergodicity of Hamiltonian Monte Carlo," *Bernoulli*, vol. 25, no. 4A, pp. 3109–3138, 2019.
- [46] S. Duane, A. Kennedy, B. J. Pendleton, and D. Roweth, "Hybrid Monte Carlo," *Physics Letters B*, vol. 195, no. 2, pp. 216–222, 1987.
- [47] L. Devlin, M. Carter, P. Horridge, P. L. Green, and S. Maskell, "The no-u-turn sampler as a proposal distribution in a sequential Monte Carlo sampler without accept/reject," *IEEE Signal Processing Letters*, vol. 31, pp. 1089–1093, 2024.
- [48] P. L. Combettes and J.-C. Pesquet, *Proximal Splitting Methods in Signal Processing*, pp. 185–212. New York, NY: Springer New York, 2011.
- [49] R. T. Rockafellar and R. J.-B. Wets, *Variational Analysis*, vol. 317 of *Grundlehren der mathematischen Wissenschaften [Fundamental Principles of Mathematical Sciences]*. Springer-Verlag, Berlin, 1998.
- [50] P. J. Green, "Reversible Jump Markov chain Monte Carlo computation and Bayesian model determination," *Biometrika*, vol. 82, pp. 711–732, 12 1995.
- [51] D. Vats, J. M. Flegal, and G. L. Jones, "Strong consistency of multivariate spectral variance estimators in Markov chain Monte Carlo," *Bernoulli*, vol. 24, no. 3, pp. 1860–1909, 2018.
- [52] T. Park and G. Casella, "The Bayesian lasso," *Journal of the American Statistical Association*, vol. 103, no. 482, pp. 681–686, 2008.
- [53] D. Donoho, "De-noising by soft-thresholding," *IEEE Transactions on Information Theory*, vol. 41, no. 3, pp. 613–627, 1995.
- [54] J. W. Smith, J. E. Everhart, W. C. Dickson, W. C. Knowler, and R. S. Johannes, "Using the ADAP learning algorithm to forecast the onset of diabetes mellitus," in *Proceedings of the annual symposium on computer application in medical care*, p. 261, 1988.
- [55] E. J. Candes and Y. Plan, "Matrix completion with noise," *Proceedings of the IEEE*, vol. 98, no. 6, pp. 925–936, 2010.
- [56] S. Gu, L. Zhang, W. Zuo, and X. Feng, "Weighted Nuclear norm minimization with application to image denoising," in *Proceedings of the IEEE conference on computer vision and pattern recognition*, pp. 2862–2869, 2014.
- [57] Z. H. Shamsi, H. S. Oh, and D.-G. Kim, "Image denoising using low rank minimization with modified noise estimation," *arXiv preprint arXiv:1504.03439*, 2015.
- [58] M. Nejati, S. Samavi, H. Derksen, and K. Najarian, "Denoising by low-rank and sparse representations," *Journal of Visual Communication and Image Representation*, vol. 36, pp. 28–39, 2016.
- [59] B. Recht, M. Fazel, and P. A. Parrilo, "Guaranteed minimum-rank solutions of linear matrix equations via nuclear norm minimization," *SIAM review*, vol. 52, no. 3, pp. 471–501, 2010.
- [60] A. Beck and M. Teboulle, "A fast iterative shrinkage-thresholding algorithm for linear inverse problems," *SIAM Journal on Imaging Sciences*, vol. 2, no. 1, pp. 183–202, 2009.